Research Internship Report

Dynamic Modelling of a Biogas-Based System for In-Situ Hydrogen Production and Electricity Generation Using SOFC

Submitted By

Aman Kumar Yadav

Bachelor of Technology

Department of Chemical Engineering and Technology

Indian Institute of Technology (BHU), Varanasi

Under the Supervision of

Prof. Sujit S. Jogwar

Associate Professor

Department of Chemical Engineering

Indian Institute of Technology Bombay

Duration: 15 May – 10 July 2025

Abstract

This project focuses on the dynamic modelling of a biogas-based system that integrates in-situ hydrogen production and electricity generation using Solid Oxide Fuel Cells (SOFCs). Building upon an existing system configuration, a dynamic model was developed to analyse the coupled behaviour of key components such as the steam reformer, SOFC stack, and combustor. The objective is to evaluate system performance under transient operating conditions and assess its potential for decentralised, sustainable energy generation.

A lumped-parameter approach was adopted, incorporating mass and energy balances along with electrochemical relations to simulate the time-dependent behaviour of the system. Open-loop simulations were conducted to study the system's response to step changes in input variables such as current demand. The results offer valuable insights into the dynamic characteristics, thermal behaviour.

Contents

Chapter 1: Introduction

1.1 Background

Biogas is a clean and locally available renewable fuel, making it suitable for sustainable energy systems. Solid Oxide Fuel Cells (SOFCs) are efficient and can run on a variety of fuels, including hydrogen produced from biogas through external reforming. Their high operating temperature allows effective thermal integration with external reformers, making them ideal for decentralised power generation.

1.2 Motivation

Hydrogen is a clean energy carrier with growing importance in sustainable systems. Producing hydrogen from biogas and using it in SOFCs improves efficiency and reduces reliance on external supply. However, these systems are thermally integrated and dynamically complex. Studying their transient behaviour is important to understand how they respond to changes in operating conditions like load or fuel flow.

1.3 Objectives and Scope of Work

The goal of this project is to develop a dynamic model of a biogas-based energy system for hydrogen production and electricity generation using Solid Oxide Fuel Cells (SOFCs). The study is based on an existing system configuration from literature.

The scope includes:

- Developing a lumped-parameter dynamic model capturing the reformer, SOFC stack, and combustor.
- Simulating open-loop behaviour to analyse the system's response to changes in input conditions.

Chapter 2: Literature Review

2.1 Key Findings

1. Why In-Situ Hydrogen Production?

One of the main challenges in hydrogen-based systems is the cost and complexity of hydrogen storage and transport. High-pressure tanks and pipelines make it difficult to scale such systems, especially in decentralised setups.

Producing hydrogen on-site through steam reforming of biogas addresses these issues by eliminating the need for external supply. It also improves overall system efficiency and makes the system more compact and practical for small or remote applications.

2. Why Solid Oxide Fuel Cells (SOFC)?[1]

Various types of fuel cells can be used for electrochemical conversion of hydrogen into water:

- Proton Exchange Membrane Fuel Cell (PEMFC)
- Phosphoric Acid Fuel Cell (PAFC)
- Molten Carbonate Fuel Cell (MCFC)
- Solid Oxide Fuel Cell (SOFC)

Each fuel cell operates under different conditions and has varying tolerance to impurities:

- **Low-temperature fuel cells** (PEMFC and PAFC):
  - Operate at approximately 60–220°C
  - Require high-purity hydrogen
  - Have very low CO tolerance (ppm-level)
- **High-temperature fuel cells** (MCFC and SOFC):
  - More tolerant to fuel impurities (e.g., CO and CO_2)

  - Better suited for integration with biogas reforming systems

Advantages of SOFC over MCFC:

- Broader operating temperature range: 600–1000°C (vs. 630–650°C for MCFC)
- Higher potential for thermal integration and cogeneration
- MCFCs suffer from:
  - Cathode dissolution
  - Gas leakage
  - Interconnection issues at high pressure

Based on these, this work focuses on:

- Integration of Steam Methane Reforming (SMR) with a Solid Oxide Fuel Cell (SOFC) for power production
- Providing opportunities for:
  - Material integration (hydrogen)
  - Energy integration (heat)

Chapter 3: Methodology

3.1 Approach

The modeling and simulation of the biogas-based SOFC system was carried out in the following manner:

- An optimized steady-state flowsheet from literature was selected as the base model for system configuration and component integration.
- A dynamic model was developed by formulating time-dependent material and energy balance equations for each unit: Steam Reformer, SOFC, Combustor, and Heat Exchanger.
- Intrinsic reaction kinetics and electrochemical relations were incorporated to accurately model component behavior.
- For the Heat Exchanger, which involves partial differential equations (PDEs), the Orthogonal Collocation Method (OCM) was applied to discretize the system spatially and convert PDEs into ordinary differential equations (ODEs).
- The resulting set of ODEs and algebraic equations was implemented in MATLAB.
- A stiff ODE solver, `ode15s`, was used for time integration to ensure numerical stability and efficiency during simulation of the dynamic system.
- Steady-state initialization was used to validate the model, and transient behavior was analyzed by perturbing key inputs.

3.2 Flowsheet Description

The system modeled in this work is based on the integrated configuration described as Configuration 2 in Georgis et al. [2]..

- Additional heat exchangers (HE1–HE3, HE5, HE7) improve energy recovery, as shown in fig 3.1

- The anodic and cathodic outlet streams from the SOFC are fed to burner, where complete combustion of CH_4, CO, and H_2 occurs.
- Air required for combustion is provided by the SOFC cathodic stream.
- The high-temperature combustor outlet stream:
  - Heats air in HE6,
  - Preheats the SOFC anode stream in HE5,
  - Supplies heat to the steam reformer (SR),
  - Heats the fuel mixture in HE3,
  - Preheats air in HE4,
  - Preheats CH_4 in HE7,
  - Generates steam in HE2 and HE1.

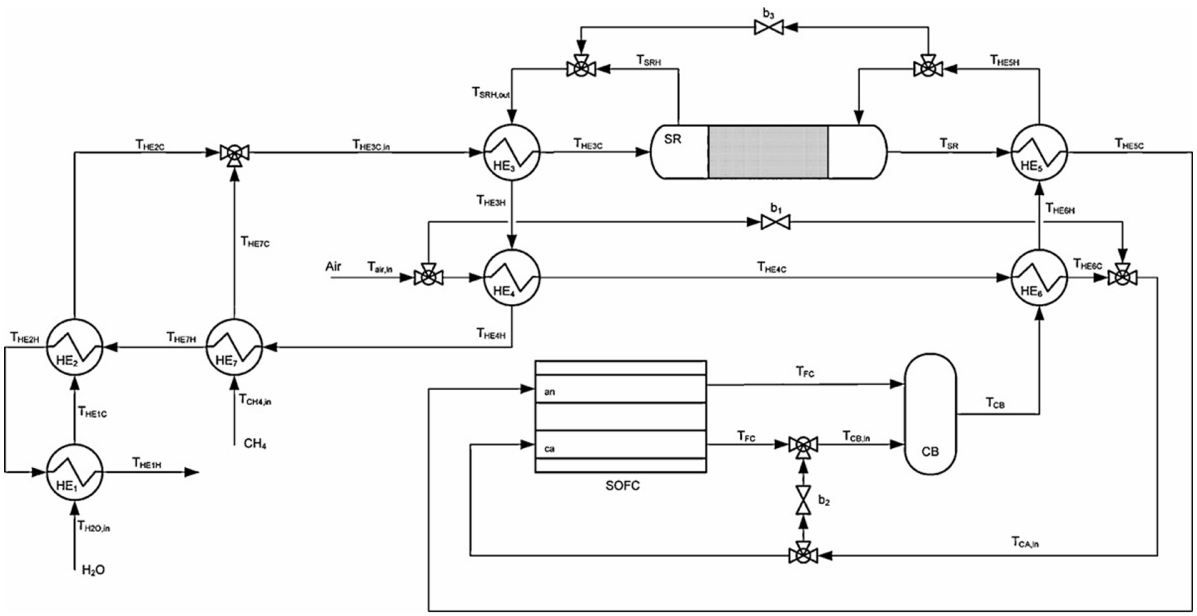

Figure 3.1: Flowsheet for study[2]

3.3 Model Development

3.3.1 Steam Reformer

The steam reformer is a catalytic reactor that facilitates the conversion of methane and steam into a hydrogen-rich gas mixture through highly endothermic reforming and shift reactions. It

serves as the primary source of hydrogen in the integrated SOFC system and requires external heat input to sustain the reforming process.

- **Chemical Reactions:**

$$\mathrm{CH_4 + H_2O \rightleftharpoons CO + 3H_2} \qquad \Delta H^{\circ}_{298} = +206.10\ \mathrm{kJ/mol}$$
$$\mathrm{CO + H_2O \rightleftharpoons CO_2 + H_2} \qquad \Delta H^{\circ}_{298} = -41.15\ \mathrm{kJ/mol}$$

  Even though the first reaction is endothermic and the second reaction is exothermic, the net system of reactions is endothermic.

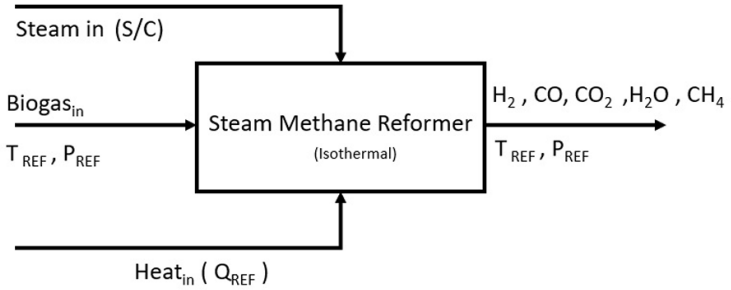

Figure 3.2: Schematic representation of Steam Reformer[1]

- **Assumptions:** Constant pressure, ideal gas behavior, lumped-parameter model, no axial dispersion.

- **Species Balances:**

$$\frac{dn_{\mathrm{CH_4}}}{dt} = \dot{n}_{\mathrm{CH_4,in}} - \dot{n}_{\mathrm{CH_4}} - m_{\mathrm{cat}} \cdot r_1 \tag{3.1}$$
$$\frac{dn_{\mathrm{H_2O}}}{dt} = \dot{n}_{\mathrm{H_2O,in}} - \dot{n}_{\mathrm{H_2O}} - m_{\mathrm{cat}} \cdot (r_1 + r_2) \tag{3.2}$$
$$\frac{dn_{\mathrm{CO}}}{dt} = \dot{n}_{\mathrm{CO,in}} - \dot{n}_{\mathrm{CO}} + m_{\mathrm{cat}} \cdot (r_1 - r_2) \tag{3.3}$$
$$\frac{dn_{\mathrm{CO_2}}}{dt} = \dot{n}_{\mathrm{CO_2,in}} - \dot{n}_{\mathrm{CO_2}} + m_{\mathrm{cat}} \cdot r_2 \tag{3.4}$$
$$\frac{dn_{\mathrm{H_2}}}{dt} = \dot{n}_{\mathrm{H_2,in}} - \dot{n}_{\mathrm{H_2}} + m_{\mathrm{cat}} \cdot (3r_1 + r_2) \tag{3.5}$$

- **Energy Balance:**

$$\frac{dT_{\mathrm{SR}}}{dt} = \frac{Q_{\mathrm{in}} - Q_{\mathrm{out}} - m_{\mathrm{cat}}(r_1\Delta H_1 + r_2\Delta H_2) + UA\Delta T_{\mathrm{LM}}}{\left(\varepsilon\rho_g C_{p,g} + (1-\varepsilon)\rho_{\mathrm{cat}} C_{p,\mathrm{cat}}\right) V} \tag{3.6}$$

$$\frac{dT_{\mathrm{jacket}}}{dt} = \frac{Q_{\mathrm{hot,in}} - Q_{\mathrm{hot,out}} - UA\Delta T_{\mathrm{LM}}}{MC_p^{\mathrm{hot}}} \tag{3.7}$$

- **Rate Expression:**[3]

$$r_1 = \frac{k_1}{p_{H_2}^{2.5}} \left(p_{CH_4} \cdot p_{H_2O} - \frac{p_{H_2}^3 \cdot p_{CO}}{K_1} \right) / (DEN)^2 \tag{3.8}$$

$$r_2 = \frac{k_2}{p_{H_2}} \left(p_{CO} \cdot p_{H_2O} - \frac{p_{CO_2} \cdot p_{H_2}}{K_2} \right) / (DEN)^2 \tag{3.9}$$

$$DEN = 1 + K_{CO} \cdot p_{CO} + K_{H_2} \cdot p_{H_2} + K_{CH_4} \cdot p_{CH_4} + \frac{K_{H_2O} \cdot p_{H_2O}}{p_{H_2}} \tag{3.10}$$

Kinetic Constants:

$$k_1 = 1.1736 \times 10^{15} \exp\left(\frac{-240.1 \times 10^3}{RT} \right) \tag{3.11}$$

$$k_2 = 5.4308 \times 10^{5} \exp\left(\frac{-67.13 \times 10^3}{RT} \right) \tag{3.12}$$

$$K_{CO} = 8.23 \times 10^{-5} \exp\left(\frac{70.65 \times 10^3}{RT} \right) \tag{3.13}$$

$$K_{H_2} = 6.12 \times 10^{-9} \exp\left(\frac{82.90 \times 10^3}{RT} \right) \tag{3.14}$$

$$K_{CH_4} = 6.65 \times 10^{-4} \exp\left(\frac{38.28 \times 10^3}{RT} \right) \tag{3.15}$$

$$K_{H_2O} = 1.77 \times 10^{5} \exp\left(\frac{-88.68 \times 10^3}{RT} \right) \tag{3.16}$$

$$K_1 = 5.75 \times 10^{12} \exp\left(\frac{-11476}{T} \right) \tag{3.17}$$

$$K_2 = 1.26 \times 10^{-2} \exp\left(\frac{4639}{T} \right) \tag{3.18}$$

- **Temperature-dependent gas densities (units: kg/m^3)**
  Assuming ideal gas behavior; P in bar, T_{SR} in Kelvin
  1. $\rho_{CH_4} = 0.717 \cdot \frac{P \cdot 298}{T_{SR}}$
  2. $\rho_{H_2O} = 0.804 \cdot \frac{P \cdot 273}{T_{SR}}$
  3. $\rho_{CO} = 1.145 \cdot \frac{P \cdot 273}{1.0133 \cdot T_{SR}}$
  4. $\rho_{CO_2} = 1.977 \cdot \frac{P \cdot 273}{1.0133 \cdot T_{SR}}$
  5. $\rho_{H_2} = 0.08988 \cdot \frac{P \cdot 273}{1.0133 \cdot T_{SR}}$
- **Temperature-dependent specific heat capacities (units: J/kg/K)**
  Each equation is a function of gas temperature T in Kelvin

1. $C_{p,\mathrm{CH_4}}(T) = (0.0032\,T + 1.3372) \cdot 1000$
2. $C_{p,\mathrm{CO}}(T) = (0.0002\,T + 0.9839) \cdot 1000$
3. $C_{p,\mathrm{CO_2}}(T) = (0.2339 \cdot \ln T - 0.4366) \cdot 1000$
4. $C_{p,\mathrm{H_2O}}(T) = 4184 \cdot (0.378278 + 1.53443 \times 10^{-4}T + 3.31531 \times 10^{-8}T^2 - 1.78435 \times 10^{-11}T^3) - 461.5$
5. $C_{p,\mathrm{H_2}}(T) = 4184 \cdot (3.56903 - 4.8950 \times 10^{-4}T + 6.22549 \times 10^{-7}T^2 - 1.19686 \times 10^{-10}T^3) - 4124$

3.3.2 Solid Oxide Fuel Cell (SOFC)

The SOFC stack consists of individual cells connected in series. A hydrogen rich stream is fed to the anodic compartment of the fuel cell, while air is supplied to the cathodic compartment.

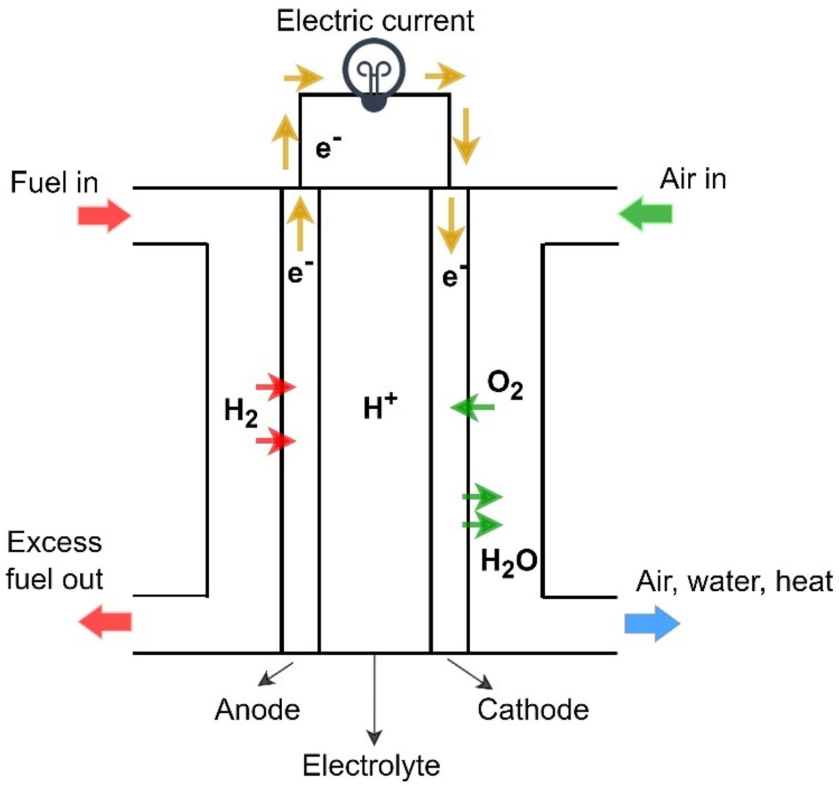

Figure 3.3: Schematic representation of SOFC[4]

- **Reactions:**

$$\text{Anode:} \quad H_2 + O^{2-} \rightarrow H_2O + 2e^-$$

$$\text{Cathode:} \quad \frac{1}{2}O_2 + 2e^- \rightarrow O^{2-}$$

$$\text{Overall:} \quad H_2 + \frac{1}{2}O_2 \rightarrow H_2O \quad ; \quad \Delta H_{\text{electrochem}} = -241.83\ \text{kJ/mol}$$

- **Output Voltage:**[5]

$$V_{\text{Cell}} = E_{\text{OCV}} - V_{\text{EEP}} - V_{\text{ASR}} \tag{3.19}$$

$$E_{\text{OCV}} = E_0 + \frac{RT}{2F} \ln\left(\frac{P_{\text{H}_2} P_{\text{O}_2}^{0.5}}{P_{\text{H}_2O}}\right) \tag{3.20}$$

$$E_0 = 1.2723 - 2.7645 \times 10^{-4} T\,[6] \tag{3.21}$$

$$V_{\text{EEP}} = \frac{RT}{2F} \ln\left(\frac{j}{j_0} + 1\right) \tag{3.22}$$

$$V_{\text{ASR}} = i R_{\text{SOFC}} \tag{3.23}$$

$$I_{\text{total}} = 2F \times n_{\text{H}_2,\text{react}} \tag{3.24}$$

$$j = \frac{I_{\text{total}}}{A} \tag{3.25}$$

$$j_0 = 0.01\, Pr_{\text{SOFC}} \exp\left(-6500\left(\frac{1}{T_{\text{SOFC}}} - \frac{1}{1123}\right)\right) \tag{3.26}$$

$$R_{\text{SOFC}} = 0.012 + 0.18 \exp\left(6500\left(\frac{1}{T_{\text{SOFC}}} - \frac{1}{1123}\right)\right) \tag{3.27}$$

$$P_{\text{SOFC}} = \eta_{\text{invr}} V_{\text{Cell}} I_{\text{total}} \tag{3.28}$$

- **Key Dynamics:**

$$\frac{dn_{\mathrm{CH_4}}}{dt} = \dot{n}_{\mathrm{CH_4,in}} - \dot{n}_{\mathrm{CH_4}} \tag{3.29}$$

$$\frac{dn_{\mathrm{H_2O}}}{dt} = \dot{n}_{\mathrm{H_2O,in}} - \dot{n}_{\mathrm{H_2O}} + \dot{n}_{\mathrm{H_2,cons}} \tag{3.30}$$

$$\frac{dn_{\mathrm{CO}}}{dt} = \dot{n}_{\mathrm{CO,in}} - \dot{n}_{\mathrm{CO}} \tag{3.31}$$

$$\frac{dn_{\mathrm{CO_2}}}{dt} = \dot{n}_{\mathrm{CO_2,in}} - \dot{n}_{\mathrm{CO_2}} \tag{3.32}$$

$$\frac{dn_{\mathrm{H_2}}}{dt} = \dot{n}_{\mathrm{H_2,in}} - \dot{n}_{\mathrm{H_2}} - \dot{n}_{\mathrm{H_2,cons}} \tag{3.33}$$

$$\frac{dn_{\mathrm{O_2}}}{dt} = \dot{n}_{\mathrm{O_2,in}} - \dot{n}_{\mathrm{O_2}} - 0.5\,\dot{n}_{\mathrm{H_2,cons}} \tag{3.34}$$

$$\frac{dn_{\mathrm{N_2}}}{dt} = \dot{n}_{\mathrm{N_2,in}} - \dot{n}_{\mathrm{N_2}} \tag{3.35}$$

$$\dot{n}_{\mathrm{H_2,cons}} = U_f \cdot \dot{n}_{\mathrm{H_2,in}} \tag{3.36}$$

$$\frac{dT_{\mathrm{SOFC}}}{dt} = \frac{1}{m_{\mathrm{SOFC}} C_{p,\mathrm{SOFC}}} \left(\sum_i \dot{n}_{i,\mathrm{in}} C_{p,i} (T_{\mathrm{in}} - T_{\mathrm{ref}}) - \sum_i \dot{n}_{i,\mathrm{out}} C_{p,i} (T_{\mathrm{SOFC}} - T_{\mathrm{ref}}) \right. \tag{3.37}$$

$$\left. - \Delta H_{\mathrm{electrochem}}\, \dot{n}_{\mathrm{H_2,react}} - I V_{\mathrm{Cell}} \right) \tag{3.38}$$

- **Model Validation**
  Initializing the model with steady state values gives flat plots. (fig. 3.4, 3.5)

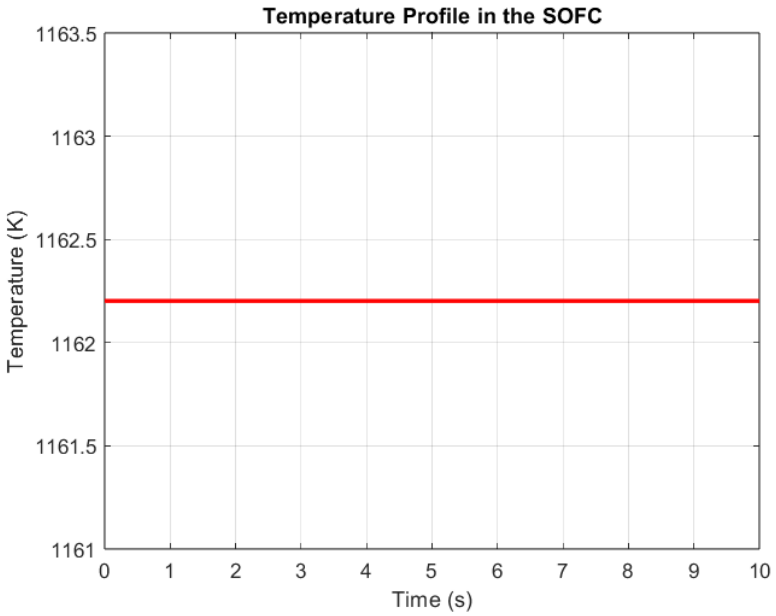

Figure 3.4: SOFC temperature versus time under steady-state initialization.

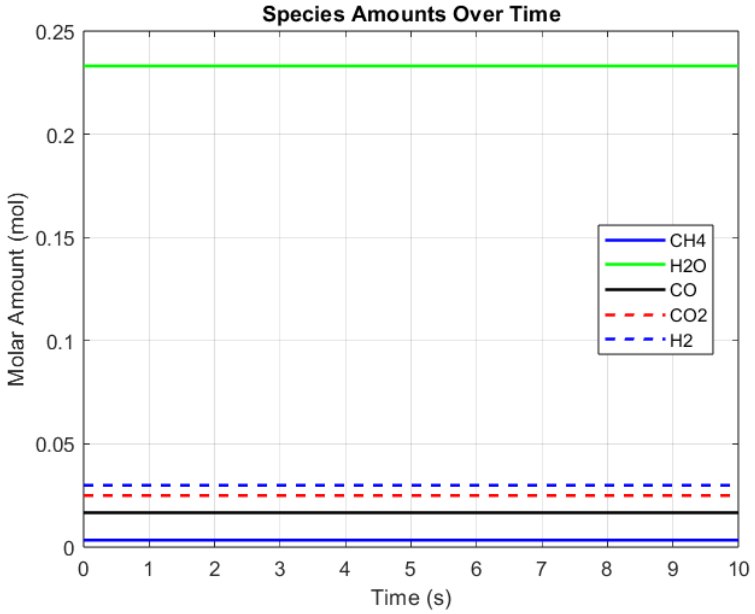

Figure 3.5: Time evolution of SOFC outlet molar flow rates for all species at steady state.

3.3.3 Combustor

The unconverted hydrogen, methane, carbon monoxide from the anode gas is burned in the combustor to increase the enthalpy of the flue gas. The cathode gas contains oxygen required for combustion.

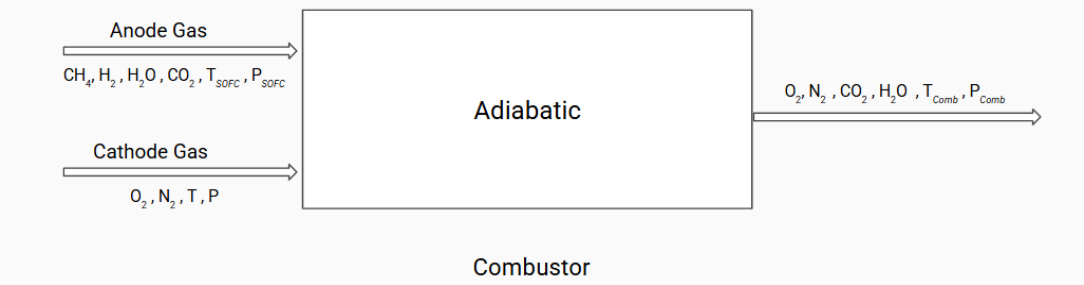

Figure 3.6: Schematic representation of the combustor

- **Reactions Involved:**

$$CH_4 + 2O_2 \rightarrow CO_2 + 2H_2O \quad ; \quad \Delta H_4, \quad \text{rate: } r_4$$

$$H_2 + \frac{1}{2}O_2 \rightarrow H_2O \quad ; \quad \Delta H_5, \quad \text{rate: } r_5$$

$$CO + \frac{1}{2}O_2 \rightarrow CO_2 \quad ; \quad \Delta H_6, \quad \text{rate: } r_6$$

- **Material and Energy balance of the combustor**

$$\frac{dn_{\mathrm{CH_4}}}{dt} = \dot{n}_{\mathrm{CH_4,in}} - \dot{n}_{\mathrm{CH_4,out}} - Vr_4 \tag{3.39}$$

$$\frac{dn_{\mathrm{H_2}}}{dt} = \dot{n}_{\mathrm{H_2,in}} - \dot{n}_{\mathrm{H_2,out}} - Vr_5 \tag{3.40}$$

$$\frac{dn_{\mathrm{O_2}}}{dt} = \dot{n}_{\mathrm{O_2,in}} - \dot{n}_{\mathrm{O_2,out}} - V\left(2r_4 + \frac{1}{2}r_5 + \frac{1}{2}r_6\right) \tag{3.41}$$

$$\frac{dn_{\mathrm{CO_2}}}{dt} = \dot{n}_{\mathrm{CO_2,in}} - \dot{n}_{\mathrm{CO_2,out}} + V(r_4 + r_6) \tag{3.42}$$

$$\frac{dn_{\mathrm{CO}}}{dt} = \dot{n}_{\mathrm{CO,in}} - \dot{n}_{\mathrm{CO,out}} + Vr_6 \tag{3.43}$$

$$\frac{dn_{\mathrm{H_2O}}}{dt} = \dot{n}_{\mathrm{H_2O,in}} - \dot{n}_{\mathrm{H_2O,out}} + V(2r_4 + r_5) \tag{3.44}$$

$$\frac{dn_{\mathrm{N_2}}}{dt} = \dot{n}_{\mathrm{N_2,in}} - \dot{n}_{\mathrm{N_2,out}} \tag{3.45}$$

$$\frac{dT_{\mathrm{comb}}}{dt} = \frac{1}{\rho_{\mathrm{comb}} C_{p,\mathrm{comb}} V_{\mathrm{comb}}}\left(\sum_i \dot{n}_{i,\mathrm{in}} C_{p,i} T_{\mathrm{in}} - \sum_i \dot{n}_{i,\mathrm{out}} C_{p,i} T_{\mathrm{comb}}\right. \tag{3.46}$$

$$\left. - \Delta H_4\, \dot{n}_{\mathrm{CH_4,react}} - \Delta H_5\, \dot{n}_{\mathrm{H_2,react}} - \Delta H_6\, \dot{n}_{\mathrm{CO,react}}\right) \tag{3.47}$$

NOTE: We will consider instantaneous reactions for methane, carbon monoxide and hydrogen.

- **Model Validation**
  Initializing the model with steady state values gives flat plots (fig. 3.7).

3.3.4 Heat Exchanger

The orthogonal collocation method is used as a numerical technique to solve the partial differential equations (PDEs) that describe the dynamic and steady-state temperature profiles of the hot and cold streams along the length of the exchanger.

Dynamic Energy Balances for Hot and Cold Fluids:

$$\frac{\partial T_H}{\partial t} = -v_H \frac{\partial T_H}{\partial z} - \frac{UA}{\rho C_p V_H}(T_H - T_C)$$

$$\frac{\partial T_C}{\partial t} = v_C \frac{\partial T_C}{\partial z} + \frac{UA}{\rho C_p V_C}(T_H - T_C)$$

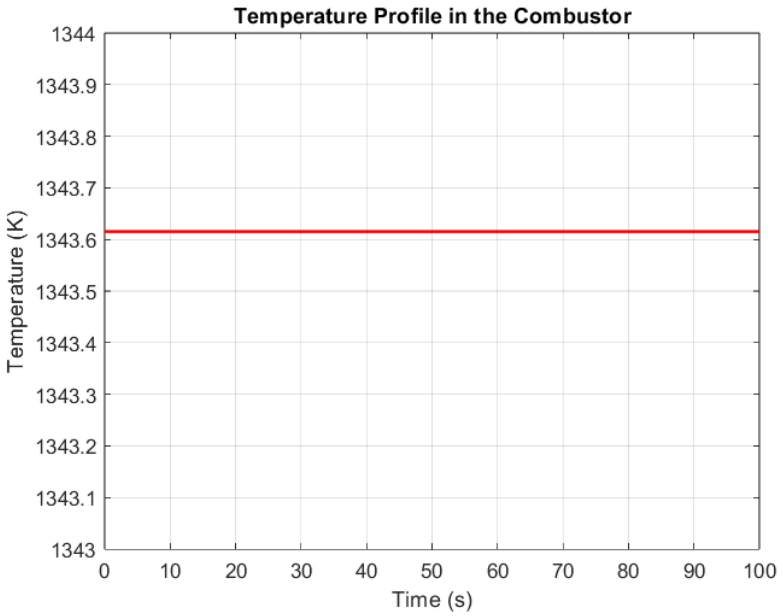

Figure 3.7: Combustor temperature versus time under steady-state initialization.

- T_H, T_C: Temperature of hot and cold fluids respectively
- v_H, v_C: Velocities of hot and cold fluids
- ρ: Fluid density, C_p: Specific heat
- V_H, V_C: Control volume of hot and cold fluid domains
- UA: Overall heat transfer coefficient times area

Example: Counter-Current Heat Exchanger (OCM)

Formulation:

$$\frac{d\mathbf{y}}{dt} = \mathbf{A_{HC}}\,\mathbf{y} + \mathbf{b_{HC}} + \mathbf{c_{HC}} \tag{3.48}$$

Where:

- $\mathbf{y}$: State vector of unknown temperatures at collocation points.
- $\mathbf{A_{HC}}$: Combined system matrix that incorporates convection, heat exchange, and spatial discretization for both hot and cold streams.
- $\mathbf{b_{HC}}$: Vector representing the contributions of the inlet temperatures $T_{H,\text{in}}$ and $T_{C,\text{in}}$ to the dynamic equations.
- $\mathbf{c_{HC}}$: Vector representing the cross-contributions of $T_{C,\text{in}}$ and $T_{H,\text{in}}$ to the dynamic equations.

Boundary Conditions:

$$T_H(0) = 100^\circ\text{C}, \qquad T_C(L) = 30^\circ\text{C}$$

Temperature Profile Along Heat Exchanger Length

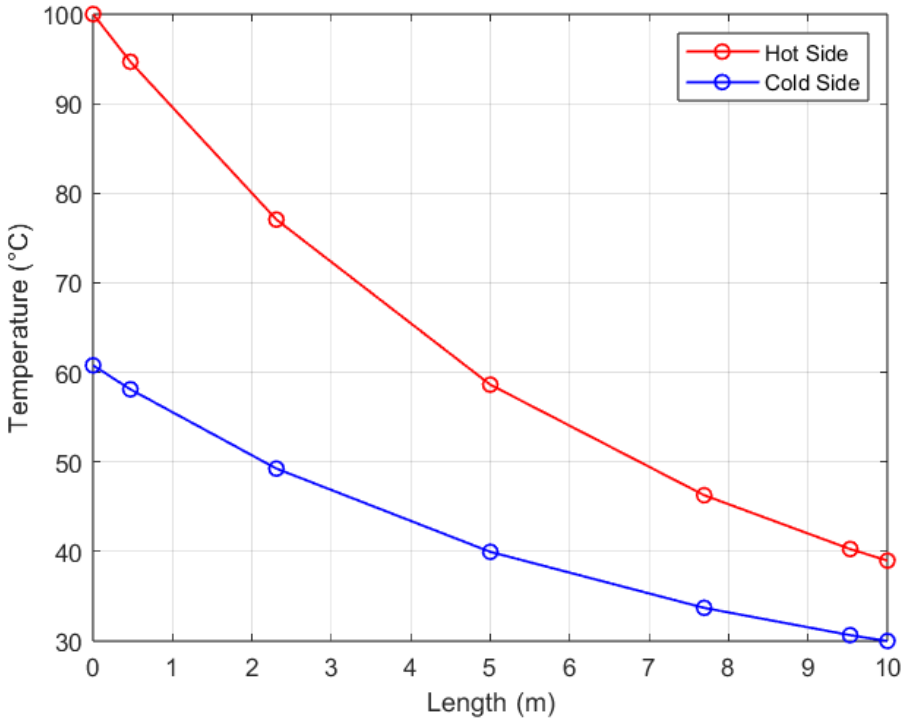

Figure 3.8: Sample temperature distribution along the length of the counter-current heat exchanger using the Orthogonal Collocation Method.

This example demonstrates the dynamic simulation and temperature profile prediction for a counter-current heat exchanger using the orthogonal collocation method (OCM) with the above parameters and boundary conditions. The collocation points table provides the spatial locations where the polynomial solution is enforced to match the PDE exactly for different discretization choices.

Symbol(s)	Description	Unit/Value
Kinetics and Thermodynamics		
p_i	Partial pressure of species i	bar
k_1	Rate coefficient for reaction 1	$\text{mol}\cdot\text{bar}^{1/2}\cdot\text{kg}_{\text{cat}}^{-1}\cdot\text{s}^{-1}$
k_2	Rate coefficient for reaction 2	$\text{mol}\cdot\text{kg}_{\text{cat}}^{-1}\cdot\text{s}^{-1}\cdot\text{bar}^{-1}$
r_1, r_2	Reaction rates for reactions 1, 2	$\text{mol}\cdot\text{kg}_{\text{cat}}^{-1}\cdot\text{s}^{-1}$
K_1	Equilibrium constant for reaction 1	bar^2
K_2	Equilibrium constant for reaction 2	Dimensionless
K_{CO}	Adsorption constant for CO	bar^{-1}
K_{CH_4}	Adsorption constant for CH_4	bar^{-1}
K_{H_2}	Adsorption constant for H_2	bar^{-1}
$K_{\text{H}_2\text{O}}$	Adsorption constant for H_2O	Dimensionless
DEN	Denominator term	Dimensionless
Reactor Geometry and Operating Conditions		
m_{cat}	Mass of catalyst	kg
L_{bed}	Length of catalyst bed	0.700 m
r_{inner}	Inner radius of bed	0.018 m
r_{outer}	Outer radius of bed	0.060 m
P_{SR}	Operating pressure of SMR reactor	1.5 bar
Catalyst and Thermal Properties		
ρ_{cat}	Density of catalyst	$2335.2\ \text{kg/m}^3$
$C_{p,\text{cat}}$	Specific heat capacity of catalyst	$444\ \text{J/(kg}\cdot\text{K)}$
ε	Void fraction of packed bed	0.4
U	Overall heat transfer coefficient	$100\ \text{J/(m}^2\cdot\text{s}\cdot\text{K)}$

Table 3.1: Summary of model parameters, symbols, and units used in the SR reformer model.

Parameter	Value / Dimension	Description
Pr_{SOFC}	atm	SOFC operating pressure
R	8.314 J·mol^{-1}·K^{-1}	Universal gas constant
A	140 m^2	SOFC effective surface area
V_{EEP}	V	Effective electrode potential
E_{OCV}	V	Open Circuit Voltage
V_{ASR}	V	Area-specific resistance losses
R_{SOFC}	Ω·cm^2	Area-specific resistance
j_0	A·cm^{-2}	Effective exchange current density
η_{invr}	0.96	DC-AC conversion efficiency

Table 3.2: Cell Voltage Parameters Used

Parameter	Value	Dimension	Description
R	8.314	J/(mol·K)	Universal gas constant
F	96485	C/mol	Faraday constant
U_f	0.8	–	Fuel utilization
$\Delta H_{\mathrm{electrochem}}$	−241.83	kJ/mol	Electrochemical enthalpy change
ρ_{SOFC}	4200	kg/m^3	SOFC density
$C_{p,\mathrm{SOFC}}$	640	J/(kg·K)	SOFC heat capacity
A	100	cm^2	Cell area
N_{cells}	384	–	Number of cells in stack
b_1, b_2, b_3	0.10	–	Bypass fractions

Table 3.3: SOFC Model Parameter

Parameter	Value	Dimension	Description
$n_{\mathrm{CH_4,in}}$	0.003388	mol/s	Methane inlet molar flow rate
$n_{\mathrm{H_2O,in}}$	0.113344	mol/s	Water inlet molar flow rate
$n_{\mathrm{CO,in}}$	0.016632	mol/s	Carbon monoxide inlet molar flow rate
$n_{\mathrm{CO_2,in}}$	0.024948	mol/s	Carbon dioxide inlet molar flow rate
$n_{\mathrm{H_2,in}}$	0.149688	mol/s	Hydrogen inlet molar flow rate
$n_{\mathrm{O_2,in}}$	0.3987864	mol/s	Oxygen inlet molar flow rate
$n_{\mathrm{N_2,in}}$	1.5011136	mol/s	Nitrogen inlet molar flow rate
$T_{\mathrm{inlet,anode}}$	973	K	Anode inlet temperature
$T_{\mathrm{inlet,cathode}}$	973	K	Cathode inlet temperature
P	101.3	kPa	Operating pressure

Table 3.4: SOFC Inlet Conditions

Parameter	Value	Dimension	Description
$n_{CH_4,out}$	0.003388	mol/s	Initial moles of methane
$n_{H_2O,out}$	0.2330944	mol/s	Initial moles of water
$n_{CO,out}$	0.016632	mol/s	Initial moles of carbon monoxide
$n_{CO_2,out}$	0.024948	mol/s	Initial moles of carbon dioxide
$n_{H_2,out}$	0.0299376	mol/s	Initial moles of hydrogen
$n_{O_2,out}$	0.3389112	mol/s	Initial moles of oxygen
$n_{N_2,out}$	1.5011136	mol/s	Initial moles of nitrogen
T_{SOFC}	1162.20	K	Initial temperature

Table 3.5: Steady-State Values for SOFC Model

Parameter	Value	Description
T_{ref}	298 K	Reference temperature
ΔH_3	−890.7 kJ/mol	Enthalpy change (CH_4 combustion)
ΔH_4	−241.83 kJ/mol	Enthalpy change (H_2 combustion)
ΔH_5	−283 kJ/mol	Enthalpy change (CO combustion)
$T_{comb,a}$	1162.20 K	Anode-side combustor temperature
$T_{comb,c}$	1142.7 K	Cathode-side combustor temperature
MC_p	36.54 J/K	Combustor Heat Capacity
$n_{CH_4,in}$	0.003388 mol/s	CH_4 inlet molar flow rate
$n_{H_2,in}$	0.0299376 mol/s	H_2 inlet molar flow rate
$n_{O_2,in}$	0.383221 mol/s	O_2 inlet molar flow rate
$n_{CO,in}$	0.016632 mol/s	CO inlet molar flow rate
$n_{CO_2,in}$	0.024948 mol/s	CO_2 inlet molar flow rate
$n_{H_2O,in}$	0.2330944 mol/s	H_2O inlet molar flow rate
$n_{N_2,in}$	1.667904 mol/s	N_2 inlet molar flow rate
C_{p,CH_4}	58.381 J/mol/K	CH_4 heat capacity
C_{p,H_2}	30.236 J/mol/K	H_2 heat capacity
$C_{p,CO}$	31.374 J/mol/K	CO heat capacity
C_{p,CO_2}	49.561 J/mol/K	CO_2 heat capacity
C_{p,H_2O}	38.459 J/mol/K	H_2O heat capacity
C_{p,O_2}	32.582 J/mol/K	O_2 heat capacity
C_{p,N_2}	31.394 J/mol/K	N_2 heat capacity

Table 3.6: Key model parameters used in the simulation of the combustor.

Parameter	**Value**	**Description**
Length of exchanger, L	10 m	Total length of the heat exchanger
Hot fluid velocity, v_H	0.1 m/s	Velocity of the hot stream
Cold fluid velocity, v_C	0.2 m/s	Velocity of the cold stream
Heat transfer coefficient, UA	30,000 W/K	Overall heat transfer coefficient
Density, ρ	1000 kg/m^3	Fluid density (both streams)
Specific heat, C_p	1000 J/kg·K	Fluid specific heat (both streams)
Control volumes, V_H, V_C	1 m^3	Volume of hot and cold sides
Inlet temperature, T_H^{in}	100°C	Hot stream inlet temperature
Inlet temperature, T_C^{in}	30°C	Cold stream inlet temperature
Collocation points	5	Number of spatial discretization points

Table 3.7: Parameters for the sample counter-current heat exchanger OCM example.

N	**Collocation Points** z_i
1	0, 0.5, 1
2	0, 0.21132, 0.78868, 1
3	0, 0.11270, 0.5, 0.88730, 1
4	0, 0.069432, 0.330009, 0.669991, 0.930568, 1
5	0, 0.046910, 0.230765, 0.5, 0.769234, 0.953090, 1
6	0, 0.033765, 0.169395, 0.380690, 0.619310, 0.830605, 0.966235, 1

Table 3.8: Collocation points z_i for different values of N in orthogonal collocation.

Chapter 4: Analysis

4.1 Small step increase in current*

To assess the dynamic behavior of the SOFC system, a small step change in current from 60.2 to 63 A is introduced during simulation.

The temperature of SOFC rises gradually (fig. 4.1(a)) due to increased heat generation from the electrochemical reaction, with the system reaching a new steady-state. Hydrogen (fig. 4.1(b)) decreases immediately due to higher consumption, while steam (fig. 4.2(b)) increases as a reaction product. Outlet molar flow rate of oxygen (fig. 4.2(a)) decreases in response to the higher current, reflecting increased cathodic consumption. Outlet molar flow rates of methane, carbon monoxide, carbon dioxide (fig. 4.2(c)), and nitrogen (fig. 4.2(d)) following a current step remains unchanged. As the current increases, the inlet temperature of the burner rises. However, the fuel supply—hydrogen and oxygen—decreases, leading to an overall drop in the burner temperature.

**the analysis refers only to the SOFC-combustor combined system.*

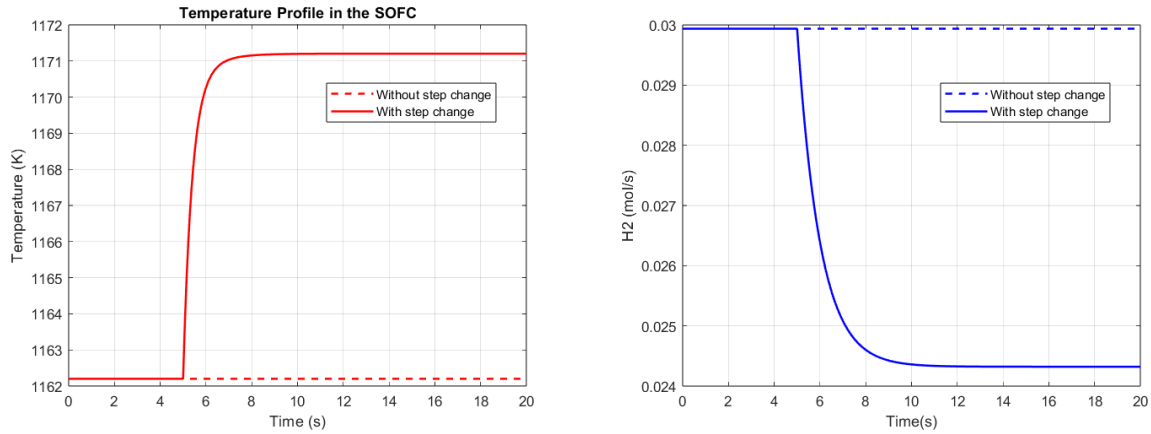

(a) Temperature of SOFC

(b) Hydrogen outlet flowrate

Figure 4.1: Small step change in current

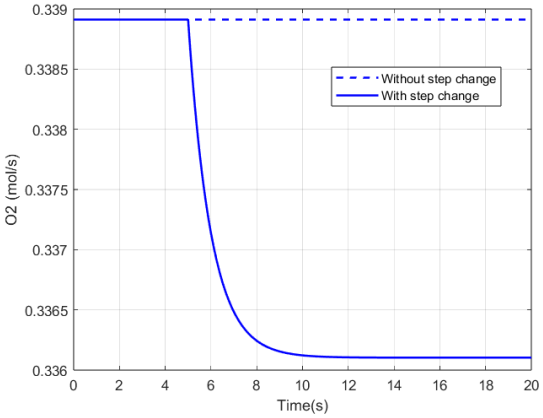

(a) Oxygen outlet flowrate

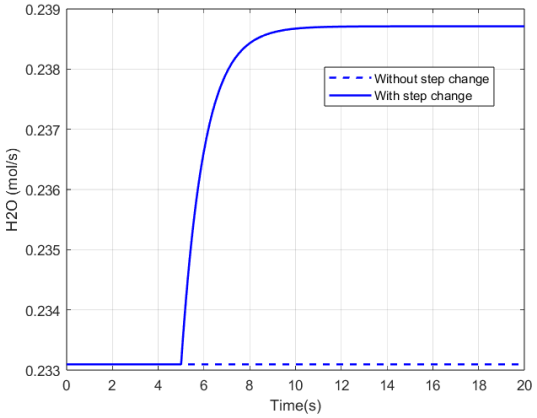

(b) Steam Outlet flowrate

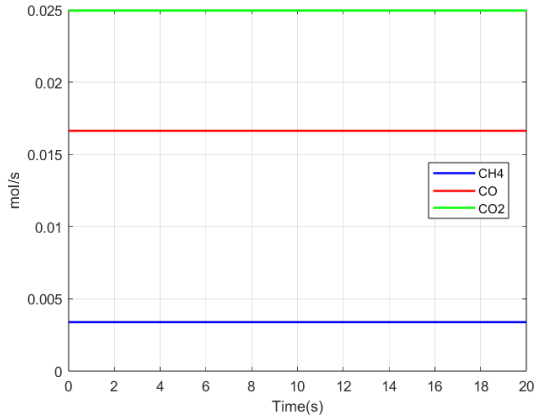

(c) Outlet molar flow rates of CH_4, CO, and CO_2

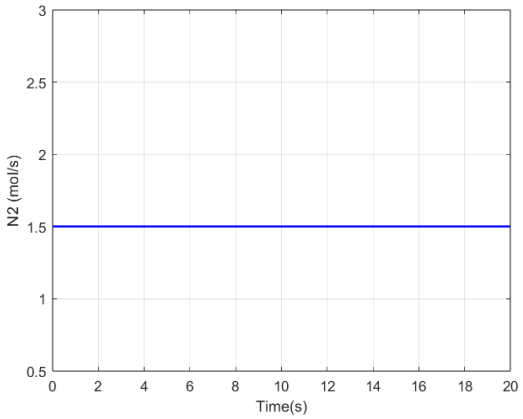

(d) Nitrogen Outlet flowrate

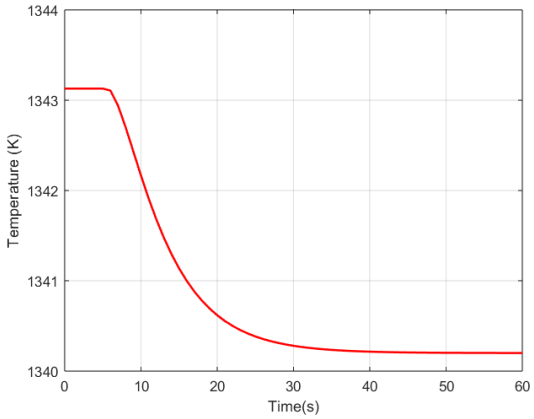

(e) Combustor temperature

Figure 4.2: Small step change in current

4.2 Large step increase in current*

To assess the dynamic behavior, a large step increase in current from 60.2 A to 70 A is introduced. The system reaches a new steady state with trends similar to those observed during a small current step.

**the analysis refers only to the SOFC-combustor combined system.*

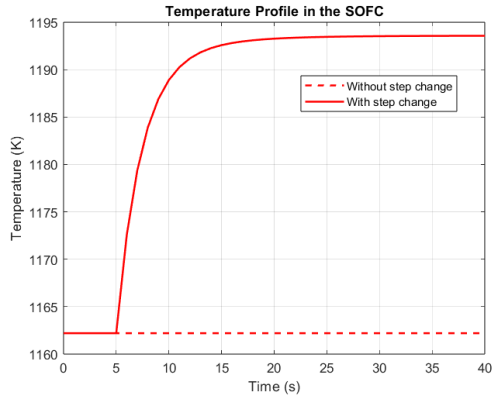

(a) Temperature of SOFC

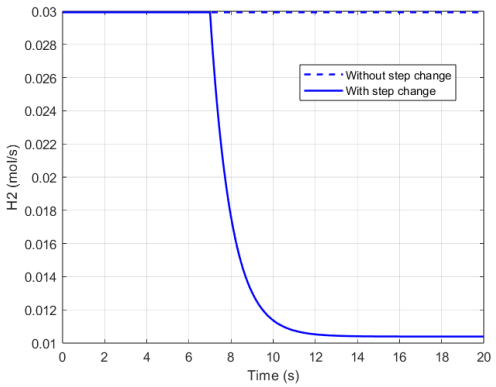

(b) Hydrogen outlet flowrate

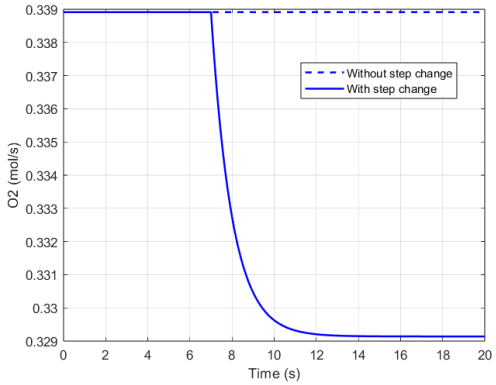

(c) Oxygen outlet flowrate

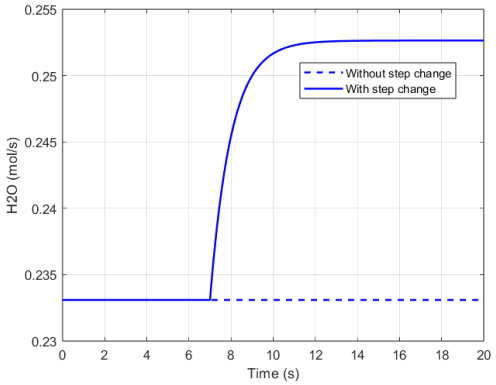

(d) Steam Outlet flowrate

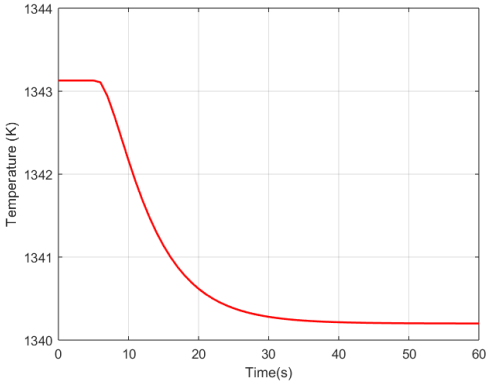

(e) Combustor temperature

Figure 4.3: Dynamic response of the SOFC-combustor system to a large step change in current.

Chapter 5: Conclusion and Future Work

5.1 Key Takeaways

The system under study utilizes an energy-integrated SOFC setup in which the anodic and cathodic outlet streams are mixed and combusted in a burner. The resulting high-temperature stream is directed through a network of heat exchangers to supply energy to various units, including the steam reformer.

When a small step increase in current (from 60.2 A to 63 A) is applied, the system exhibits stable open-loop dynamics. The increase in current leads to higher hydrogen consumption and greater heat generation within the SOFC, causing a gradual rise in fuel cell temperature. However, due to reduced availability of unreacted hydrogen and oxygen, the heat release in the burner decreases. This results in lowering the burner outlet temperature. Nevertheless, the system successfully stabilizes at a new steady state without exhibiting any instability, demonstrating its robustness to small disturbances.

In the case of a larger current step (from 60.2 A to 70 A), the system continues to maintain stable open-loop behavior. System reaches a new steady state with trends similar to the small-step case, confirming its ability to handle large disturbances without compromising operational safety.

In summary, the system demonstrates excellent open-loop stability under both small and large disturbances in current.

5.2 Limitations and Scope

While the open-loop analysis of the system provides valuable insights into its dynamic behavior, several limitations and assumptions must be acknowledged:

- **Subsystem-Level Analysis:** The analysis was limited to the SOFC-combustor combination. Other major components of the complete energy-integrated system—such as the steam reformer and heat exchangers—were not included. As a result, interactions between these units and their influence on overall system dynamics were not captured.

- **Lumped Parameter Model:** The system is modeled using a lumped parameter approach, assuming uniform properties throughout each unit. This may overlook spatial variations in temperature, concentration, and reaction rates.
- **Neglect of Degradation Effects:** Long-term degradation mechanisms such as material aging, electrode poisoning, and thermal stress effects have not been considered, which can impact real-world performance.
- **Ideal Operating Conditions:** The analysis assumes ideal gas behavior and constant physical properties, which may differ from actual operating conditions.
- **No Control Strategy Applied:** This study focuses solely on open-loop behavior. The absence of a control system means the model does not account for feedback stabilization under real-time load changes or disturbances.
- **Limited Range of Disturbances:** Only step changes in current were considered. Other dynamic inputs such as ramp changes, periodic variations, or stochastic disturbances were outside the scope of this study.

Bibliography

[1] V. Uday and S. S. Jogwar, "Optimal design of an integrated biogas-based fuel cell system," *Industrial & Engineering Chemistry Research*, vol. 63, no. 10, pp. 4496–4508, 2024.

[2] D. Georgis, S. S. Jogwar, A. S. Almansoori, and P. Daoutidis, "Design and control of energy integrated sofc systems for in situ hydrogen production and power generation," *Computers Chemical Engineering*, vol. 35, no. 9, pp. 1691–1704, 2011. Energy Systems Engineering.

[3] J. Xu and G. F. Froment, "Methane steam reforming, methanation and water-gas shift: I. intrinsic kinetics," *AIChE Journal*, vol. 35, no. 1, pp. 88–96, 1989.

[4] J. Y. Tan, R. M. T. Raja Ismail, and M. S. Jadin, "Dynamic model and robust control for the pem fuel cell systems," *Results in Engineering*, vol. 22, p. 102247, 2024.

[5] N. S. Siefert and S. Litster, "Exergy economic analysis of biogas fueled solid oxide fuel cell systems," *Journal of Power Sources*, vol. 272, pp. 386–397, 2014.

[6] P. Lisbona, A. Corradetti, R. Bove, and P. Lunghi, "Analysis of a solid oxide fuel cell system for combined heat and power applications under non-nominal conditions," *Electrochimica Acta*, vol. 53, no. 4, pp. 1920–1930, 2007. POLYMER ELECTROLYTES Selection of papers fromThe 10th International Symposium (ISPE-10)15-19 October 2006, Foz do Iguaçú-PR, Brazil.